Nanoscale

RSC Publishing

PAPER

View Article Online
View Journal | View Issue

Cite this: *Nanoscale*, 2013, **5**, 11692

Redox responsive nanotubes from organometallic polymers by template assisted layer by layer fabrication†

Jing Song,[a] Dominik Jańczewski,[a] Yuanyuan Guo,[b] Jianwei Xu[a] and G. Julius Vancso*[b]

Received 29th July 2013
Accepted 3rd September 2013

DOI: 10.1039/c3nr03927g

www.rsc.org/nanoscale

Redox responsive nanotubes were fabricated by the template assisted layer-by-layer (LbL) assembly method and employed as platforms for molecular payload release. Positively and negatively charged organometallic poly(ferrocenylsilane)s (PFS) were used to construct the nanotubes, in combination with other polyions. During fabrication, multilayers of these polyions were deposited onto the inner pores of template porous membranes, followed by subsequent removal of the template. Anodized porous alumina and track-etched polycarbonate membranes were used as templates. The morphology, electrochemistry, composition and other properties of the obtained tubular structure were characterized by fluorescence microscopy, scanning (SEM) and transmission electron microscopy (TEM) and energy-dispersive X-ray (EDX) spectroscopy. Composite nanotubes, consisting of poly(acrylic acid) anions with PFS^{+} and nanoparticles including fluorophore labelled dextran and decorated quantum dots, with PFS polyelectrolytes were also fabricated, broadening the scope of the structures. Cyclic voltammograms of PFS containing nanotubes showed similar redox responsive behaviour to thin LbL assembled films. Redox triggered release of labelled macromolecules from these tubular structures demonstrated application potential in controlled molecular delivery.

Introduction

Nanomaterials exhibiting tubular morphology have drawn substantial scientific interest since the discovery of carbon nanotubes in 1991.[1] Nanotubes have large interfacial areas, tunable size dependent properties and anisotropic properties.[2–5] The inner and outer surface of the nanotube can be functionalized independently enabling applications in catalysis, photonics, and sensors.[5–12] Due to the open end of their tubular structures, the nanotubes can encapsulate and release large amounts of target molecules, and persist for a long circulation time in the blood stream.[13,14] As such, nanotubes have high potential for drug and gene delivery, particularly when transport through cell membrane is required.[15,16] To date, a number of methods have been used to prepare nanotubes made of carbon, metals, metal oxides, semiconductors and polymeric materials.[5,17–21] The template assisted method, pioneered by Martin, provided a simple and effective way to fabricate micro- and nanotubes;[22,23] it is applied in combination with various deposition techniques such as electroless plating, sol–gel, chemical vapor deposition and layer by layer (LbL) deposition[24–27] which are frequently used to prepare polyelectrolyte nano objects in aqueous solutions. The sequential LbL deposition technique exploits the electrostatic attraction between oppositely charged species in a porous membrane template.[3,28–31] For example, the positively charged polyallylamine hydrochloride (PAH) and the negatively charged poly(acrylic acid) (PAA) nanotubes were obtained by alternate exposure of the template membrane to the PAH and PAA polyelectrolyte solutions.[32] LbL is also used to prepare human serum albumin or cytochrome C protein nanotubes for applications such as biosensors and enzymatic bioreactors.[19,33,34] A diversity of nanotube functions can be accomplished by assembling different kinds of components or by introducing functional groups on the surface of the structures.[2,35–38] Various types of templates can also be employed to achieve diversity in shape and morphology. For example, composite tubular nanostructures prepared by deposition of polyelectrolyte multilayers on electrospun nanofibers or on single carbon nanotubes have been fabricated for nanodevice applications.[22,39]

Nevertheless, there are limited reports on construction and application of stimuli responsive nanotubes. Cohen *et al.* demonstrated reversible swelling–deswelling of substrate-bound nanotube arrays in response to the pH stimulus.[40] Such

[a]*Institute of Materials Research and Engineering, A*STAR (Agency for Science, Technology and Research), Research Link 3, 117602, Singapore*

[b]*MESA+ Institute for Nanotechnology, Materials Science and Technology of Polymers, University of Twente, P.O. Box 217, 7500 AE Enschede, The Netherlands. E-mail: g.j.vancso@utwente.nl; Fax: +31 53 4893823; Tel: +31 53 489 2974*

† Electronic supplementary information (ESI) available: Nanotube wall thickness determination protocol. See DOI: 10.1039/c3nr03927g

geometry changes can be used for systematic variation in mechanomutability and can have applications as a dynamic substrate.[41] Compared to other stimuli, such as pH,[42,43] temperature,[44] light,[45,46] or magnetic field,[47] the redox response can be controlled in an easy and precise way.[48]

The utility of poly(ferrocenylsilane)s (PFS), which contain a main chain with alternating ferrocene and silicone units, as a redox responsive polymer, has been shown in a number of articles.[49,50] Shell cross-linked organometallic nanotubes have been synthesized by self-assembly of PFS-*b*-PMVS block copolymers and are used for control and regulation of one dimensional arrays of silver nanoparticles formation.[51] PFS polyions with both positive and negative charges can, for example, be derived from iodopropyl precursors.[52] In our previous studies, we presented hollow capsules and composite micelles made of PFS polyions by using LbL deposition, as redox controlled delivery agents.[53–55] Multilayers prepared on a flat substrate were used for surface mediated molecular delivery application.[56,57] The water soluble PFS multilayers prepared by other groups have been used in tuning the optical properties of photonic crystals with nanometer scale precision.[58] Also a redox tunable defect embedded in a colloidal photonic crystal was employed for reversible tuning of an intragap transmitting state.[59] In this paper, we report on the fabrication and characterization of a new type of redox stimulus responsive nanotube, fabricated from PFS, using the LbL template assisted technique. pH responsive polyions (PAA^-) and surface functionalized quantum dots (QDs) were also incorporated into these structures to prove the versatility of the established protocols. The application potential of these nanotubes as a controlled, redox triggered, delivery nanodevice is illustrated by redox controlled release of fluorescence guest molecules.

Experimental

Materials

Poly(ethyleneimine) (PEI, $M_w = 2.5 \times 10^4$ g mol^{-1}), poly(acrylic acid) (PAA, $M_w = 4.5 \times 10^5$ g mol^{-1}), 3-mercapto-1-propanesulfonate, 3-aminopropyltrimethoxysilane, sodium perchlorate, and sodium hydroxide were obtained from Aldrich and used as received. The fluorescence dye-labelled dextran employed in this study, Alexa Fluor®488 (Dextran-Alexa 488) ($M_w = 1 \times 10^5$ g mol^{-1}), was purchased from Invitrogen (Carlsbad, USA). Porous alumina templates with an average pore size of 200 nm and a pore depth of 60 μm were obtained from Whatman (Clifton, USA). The track etched polycarbonate PC membrane used (Isopore membrane, 25 mm, pore diameter, 400 nm, pore depth, 20 μm) was purchased from Millipore Corp (Danvers, USA).

PFS synthesis

Positively (PFS^+) and negatively (PFS^-) charged polymers with $M_w = 1.67 \times 10^4$ g mol^{-1}, PDI = 1.3 were synthesized by ring opening polymerization (ROP) of strained, chlorinated cyclopherocenophane followed by side group modification as described previously.[52]

Preparation of QD solution

CdSe–ZnS core–shell nanocrystals coated with trioctylphosphine oxide–*n*-hexadecylamine ligands, with emission at 570 nm, were synthesized and transferred into water using an amphiphilic polymer as previously described.[60,61] 2 mg of an amphiphilic polymer for 1 mg of QDs were used resulting in a suspension of 20 mg mL^{-1} of negatively charged, carboxylic surface functionalized QDs.

Nanotube fabrication

Porous polycarbonate membranes (PC) and anodized alumina substrates (AAO) were employed as templates for nanotubes fabrication. Two types of membranes were employed, *i.e.*, PC with a pore diameter of $\phi = 400$ nm, a thickness of $h = 20$ μm, and an aspect ratio of 1 : 50; and AAO with a pore diameter of $\phi = 200$ nm, a thickness of $h = 60$ μm, and an aspect ratio of 1 : 300. Polycarbonate membranes were treated with 3-aminopropyltrimethoxysilane in a vacuum desiccator at room temperature for three hours to render the surface positively charged. To achieve the same effect, porous alumina substrates were immersed in PEI solutions (1 mg mL^{-1}) for 1 hour. The modified substrates were dipped sequentially in aqueous PFS polyanion and polycation solutions (1 mg mL^{-1}, 0.5 M NaCl) for 10 minutes, respectively, rinsed twice with deionized water (2 min each step) and dried with a stream of nitrogen between each deposition step. The same procedure was used to fabricate composite nanotubes using PAA. Guest molecules, modified quantum dots and dextran coupled Alexa 488 dye molecules were incorporated into nanotubes as the last step of the sequential assembly, *i.e.* they formed a decorative, inner layer.

To selectively remove the excessive thin polymer films deposited at the template surface, the top and the bottom of the membrane was plasma treated in Ar for 10 min (AAO membrane) and in O_2 for 15 s (PC membrane). To accomplish a final tubular structure, the PC membrane was dissolved in dichloromethane, while the alumina template was removed by KOH (1 M) solution. Tubes fabricated in an AAO membrane were purified by two centrifugation and washing steps followed by subsequent dialysis against MilliQ water for 3 days (Spectra/Por 4 membrane). An aqueous dispersion containing some yellow precipitants was obtained in this way. The product obtained with PC membranes was purified by several dichloromethane washing and centrifugation cycles followed by redispersion in ethanol.

Characterization

Cyclic voltammetry measurements were carried out using an Autolab PGSTAT 302N (Metrohm, Utrecht, the Netherlands) potentiostat employing a three-electrode configuration. The ITO substrates, with the deposited nanotubes, acted as the working electrode, Pt as the reference electrode, and Pt wire as the counter electrode. 0.1 M $NaClO_4$ solution was used as the supporting electrolyte. To improve the nanotube attachment, a negative charge was introduced onto the cleaned ITO surface by immersion into 3-mercapto-1-propanesulfonate (~0.1 mM) solution. Prior to the measurements, oxygen was removed from

the electrochemical cell by passing nitrogen through the electrolyte solution for 5 min. A series of cyclic voltammograms holding the oxidation potentials at 0.7 V *vs.* Pt and using varying time intervals were recorded.

Samples for scanning electron microscopy (SEM) were prepared by applying a drop of tubular material suspension onto a glass slide followed by vacuum drying. After sputtering with gold, the samples were observed using a SEM (JSM5600LV, JEOL, Tokyo, Japan) at an operating voltage of 10 keV. Transmission electron microscopy (JEOL JEM-2010F FasTEM) and energy-dispersive X-ray (EDX) measurements were recorded at 100 kV. For TEM the samples were prepared by direct deposition of aqueous solution drops onto the copper grids, which were coated in advance with supportive Formvar films and carbon (Agar Scientific). The samples were dried for 8 hours at room temperature before imaging.

Florescence imaging experiments were carried out using a Wide-Field Microscope (WFM) based on a Nikon ECLIPSE Ti–U inverted microscope frame. Light from a continuous wave (CW) multi-line Ar laser was fiber-coupled to a Nikon TIRF attachment and focused on the back aperture of a high numerical aperture objective (Nikon TIRF Apo, 100×, NA = 1.49, oil immersion). The luminescence light was collected by the same objective and after passing through the dichroic and emission filters it was directed to an iXonEM+897 EMCCD camera connected to the side port of the microscope. Immersion oil was added between the objective and the cover slip for index matching.

Controlled release of guest molecules

PFS nanotubes loaded with dye molecules were suspended in 5 mL of 0.1 M NaCl electrolyte solutions. The as-obtained suspension of PFS tubes was exposed to electrochemical oxidizing potential (0.9 V *vs.* Pt) using an Autolab PGSTAT 302N (Metrohm, Ultrecht, the Netherlands) potentiostat in a three electrode configuration. ITO coated glass slides were used as the working electrode, Pt wire was used as the reference electrode, and a Pt plate was used as the counter electrode. At defined time intervals, 1.5 mL of the solution was withdrawn and purified by centrifugation. The release of guest molecules was followed by observation of fluorescence changes of the supernatant.

Results and discussion

Redox responsive nanotube fabrication

Cylindrical nanotubes with uniform diameter and length were constructed using the template-assisted layer-by-layer fabrication technique. Redox active polyelectrolytes (PFS) and other polymeric components served as construction materials (Table 1). The length and the outer diameter of the nanotubular assemblies were defined by the template dimensions. The wall thickness and the inner diameter of the tubes were precisely controlled by changing the number of deposited polyelectrolyte layers. The nanotube fabrication procedure is illustrated in Scheme 1.

Table 1 provides a summary of the nanotubes composition, the template employed and (when applicable) the type of the encapsulated cargo.

Upon polymer deposition the original white substrate turned yellow (characteristic color of PFS), giving evidence for the successful LbL assembly. In all experiments, LbL deposition occurred simultaneously on the inner wall of the template surface and at the top and bottom of the membrane between the openings of nanopores. After surface layer removal, the SEM images of PFS 5 bilayers coated PC and alumina membranes are shown in Fig. 1a and b. The distribution of pore sizes was determined from SEM images after each deposition cycle (Table 2).

Differences between inner diameter values in subsequent deposition steps were used to determine the average bilayer thickness (see ESI†). The average layer thickness determined from PC and AAO membranes was 6 nm (±10%) and 3 nm (±9%), respectively. The observed values are similar to the thickness we obtained for the same materials on flat substrates (4.5–5 nm) under the same experimental conditions.[56]

Fabricated nanotubes were visualized using an electron microscope. SEM images of PFS nanotubes [$(PFS^-/PFS^+)_{pc}$, $(PFS^-/PFS^+)_{Al}$] with different aspect ratio values obtained from PC and AAO templates respectively are shown in Fig. 1c and d. Well-defined tubular structures can be observed. The outer diameter of the nanotubes can be estimated to be about 400 nm (PC template) and 200 nm (AAO template), which correspond to the pore diameters of the original membranes. From a series of SEM images, we estimated the total length of the nanotubes. The

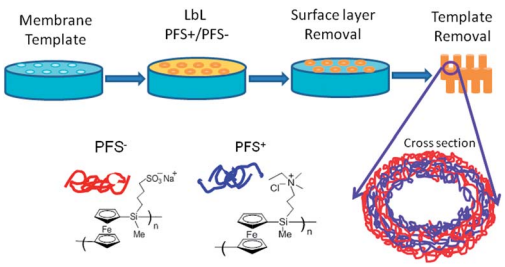

Scheme 1 LbL assembly of redox polyelectrolyte nanotubes.

Table 1 Summary of nanotube composition

Sample ID	Polyanion	Polycation	Bilayer number	Template	Encapsulated cargo
$(PFS^-/PFS^+)_{pc}$	PFS^-	PFS^+	5	PC	—
$(PFS^-/PFS^+)_{Al}$	PFS^-	PFS^+	5	Al_2O_3	—
$(PAA^-/PAH^+)_{pc}$	PAA^-	PAH^+	5	PC	—
$(PAA^-/PFS^+)_{Al}$	PAA^-	PFS^+	5	Al_2O_3	—
$(PFS^-/PFS^+)_{Al}$-QD	PFS^-	PFS^+	5	Al_2O_3	QD
$(PFS^-/PFS^+)_{Al}$-Alexa	PFS^-	PFS^+	5	Al_2O_3	Alexa 488

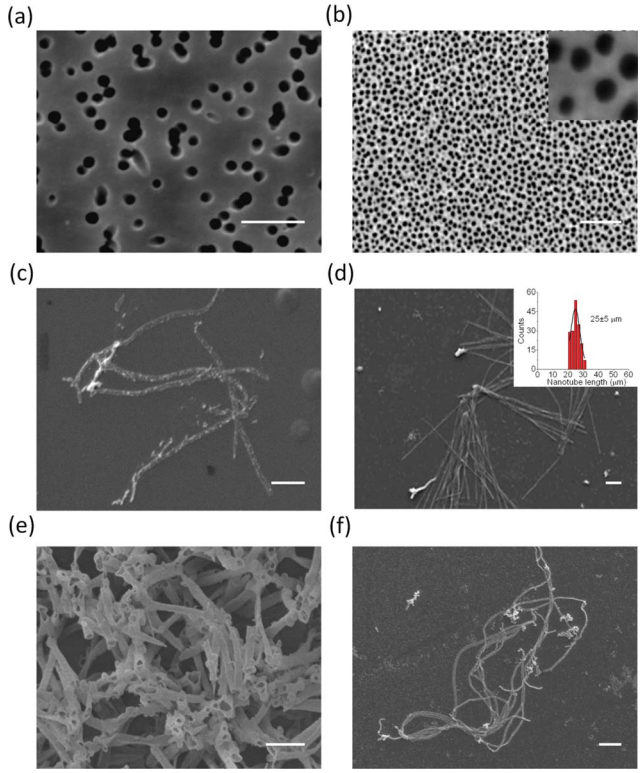

Fig. 1 SEM micrographs of (a) $(PFS^-/PFS^+)_5$ coated PC membrane; (b) $(PFS^-/PFS^+)_5$ coated alumina membrane; (c) $(PFS^-/PFS^+)_{pc}$ tubes obtained from the PC template; (d) $(PFS^-/PFS^+)_{Al}$ tubes obtained from the AAO template; (e) $(PAA^-/PAH^+)_{pc}$ tubes obtained from the PC template; (f) $(PAA^-/PFS^+)_{Al}$ tubes obtained from the AAO template. Scale bar = 2 μm for all images.

Table 2 Inner pore diameter (nm) as a function of bilayer number

Bilayer number	0	1	2	3	4	5
AAO (nm)	210 ± 20	204 ± 16	198 ± 21	192 ± 19	188 ± 20	184 ± 19
PC (nm)	404 ± 46	390 ± 43	377 ± 42	365 ± 41	352 ± 39	340 ± 41

observed values obtained are about 10 ± 3 μm (aspect ratio 1 : 25) for $(PFS^-/PFS^+)_{pc}$ and 25 ± 5 μm (aspect ratio 1 : 125) for $(PFS^-/PFS^+)_{Al}$. The $(PFS^-/PFS^+)_{Al}$ tube length distribution is shown in the inset of Fig. 1d. Nanotubes shorter than the original thickness of the membranes, as achieved in all experiments, could be the result of the defects in the original templates. Following the same method, but using different polymers, pH responsive nanotubes $(PAA^-/PAH^+)_{pc}$ and $(PAA^-/PFS^+)_{Al}$ were fabricated from PC and AAO membranes, respectively (Fig. 1e and f).

The tubular structure and composition of nanotubes were also confirmed by transmission electron microscopy (TEM) (Fig. 2) and characterized by energy dispersive X-ray (EDX) measurements. The analysis of PFS nanotubes by energy dispersive X-ray (EDX) spectroscopy showed the presence of C, Si, Fe as material components. The expected ratio of the elements Fe : Si ≈ 1 : 1 from PFS is observed. Signals of other elements are originating most likely from the TEM copper grids.

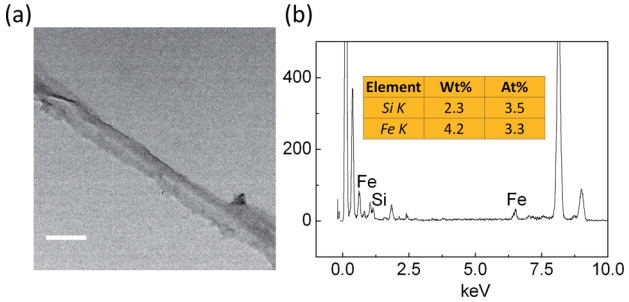

Fig. 2 (a) TEM image of the $(PFS^-/PFS^+)_{pc}$ tube obtained from a PC template, scale bar = 0.5 μm. (b) EDX spectrum of the tubular structure.

Redox properties of PFS^-/PFS^+ nanotubes

Cyclic voltammetry (CV) was employed to investigate the redox activity of the nanotubes. The samples were prepared by placing a drop of aqueous nanotube dispersion on the top of an ITO electrode followed by drying under vacuum. As shown in Fig. 3, two types of nanotubes $(PFS^-/PFS^+)_{Al}$ and $(PAA^-/PFS^+)_{Al}$ with 5 bilayers were investigated. Voltammetry experiments were carried out at a scan rate of 50 mV s^{-1} in a 0.1 M $NaClO_4$ supporting electrolyte. PFS nanotubes and PFS composite nanotubes do not prevent electron transfer of redox active ferrocene units.[56] Two reversible oxidation waves, characteristic of the PFS polymer, were observed.[56,57,62] However, the two oxidation waves of composite nanotubes $(PAA^-/PFS^+)_5$ are less distinguishable than $(PFS^-/PFS^+)_5$ nanotubes. The oxidation potential of $(PAA^-/PFS^+)_{Al}$ shifts to higher values compared to $(PFS^-/PFS^+)_{Al}$. The interpenetration of a non-redox active (PAA^-) and a redox active polymer chain (PFS^+) may influence the rate of electron transfer.

Nanotubes with nanoparticles and dye molecules

Utilization of the template assisted LbL process can be extended to yield different inner and outer surface structures and compositions of the nanotubes. Various fabrication approaches have been employed to assemble building blocks such as polymers, nanoparticles, proteins, inorganic and organic functional molecules by sequential assembly.[2] The LbL assembly of

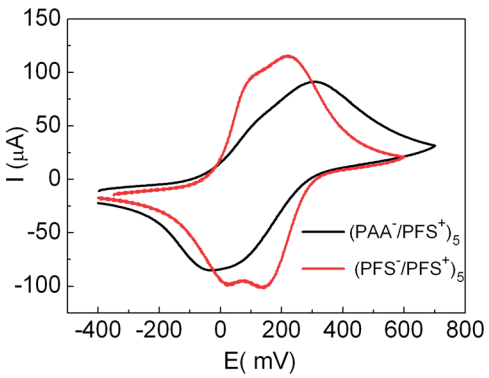

Fig. 3 Typical cyclic voltammograms of synthesized nanotubes. Experiments were carried out in 0.1 M $NaClO_4$ aqueous solution using a Pt reference electrode and a Pt counter electrode at a constant scan rate of 50 mV s^{-1}.

inorganic particles into smart multilayers provides the opportunity to combine the electronic, optical, and magnetic properties of inorganic nanostructures with unique responses of macromolecules. In our experiments, quantum dots (QDs) exhibiting narrow emission bandwidth, photochemical stability, and high quantum yield have been incorporated into the walls of the nanotubes. Following previously published procedures,[60,61] hydrophobic CdSe–ZnS QDs were micellized with polymeric coating to form negatively charged assemblies. Such negatively charged QDs were subsequently incorporated into multilayer systems as the last, inner decorative layer. Fig. 4a shows the fluorescence image of QD labeled PFS nanotubes ($(PFS^-/PFS^+)_{AI}$-QD). The intensity distribution of single fluorescent nanotube is demonstrated in the inset image, indicating the maximum of fluorescence located within the nanotube structure. The QD particles were confirmed to be well distributed along the nanotube. The same strategy was extended to the organic dye molecules, dextran labeled Alexa 488. The negative charged Alexa 488 was used as a functional building block through the deposition on the last layer of PFS^+. The fluorescence images of dye labeled PFS nanotubes ($(PFS^-/PFS^+)_{AI}$-Alexa) and the intensity distribution of single fluorescent nanotube are shown in Fig. 4c and d.

Molecular delivery application

The open ends and the large specific surface area make nanotubes good candidates for molecular delivery applications.[11] Nanotubes can be readily loaded with large quantities of guest species and provide a large surface area of release. Additionally, redox active nanotubes may provide controlled release profiles compared to inert, non-responsive structures. In our experiments dye labeled dextran was deposited onto the inner wall of the nanotubes and the electrochemical potential (0.9 V *vs.* Pt wire) was applied to induce redox driven tube disassembly. The accumulated release of the guest molecules, monitored using a fluorescence spectrometer as a function of electrolysis time, is shown in Fig. 5. After 15 hours of electrolysis, the fluorescence of the solution reaches saturated levels, indicating the end of the release process. Similar exponential release profiles were observed when guest molecules, embedded into multilayer thin films, were investigated.[57] The dye release rate from nanotubes is slower compared to flat thin films;[57] however the mechanism of release remains likely similar. During the oxidation process of PFS, positive charges are introduced to the ferrocene units in the PFS main chain. The presence of additional charges results in charge imbalance and electrostatic repulsion, which are the main causes for the tube disassembly.

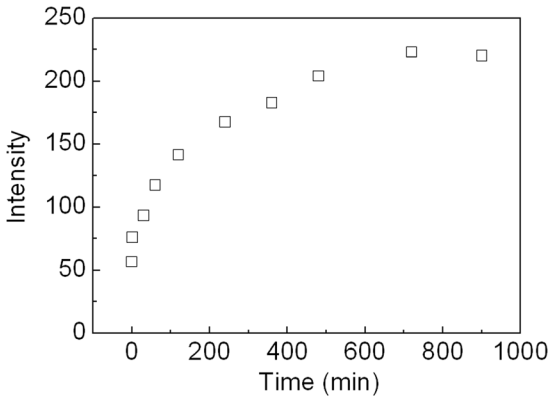

Fig. 5 Release profile of dye molecules upon electrochemical oxidation of $(PFS^-/PFS^+)_{AI}$-Alexa bilayer nanotubes (Alexa 488 was encapsulated in the inner layer, aging took place at 0.9 V *vs.* Pt). Fluorescence of a supernatant was measured upon removal of tubes by centrifugation.

Despite the fact that the dye used was decorated on the inner surface of the tube, there are no signs of sudden release of the guest molecules from the tube structure in solution. This could be associated with the strong binding of dyes with PFS *via* electrostatic forces. As such, rather substantial PFS tube disintegration is necessary to observe a free, non-bound dye in the supernatant. This hypothesis was confirmed by the presence of small broken pieces of the nanotubes visible in the SEM image at half stage of electrolysis experiment (Fig. 6). Moreover at the end of electrolysis experiment, there were no

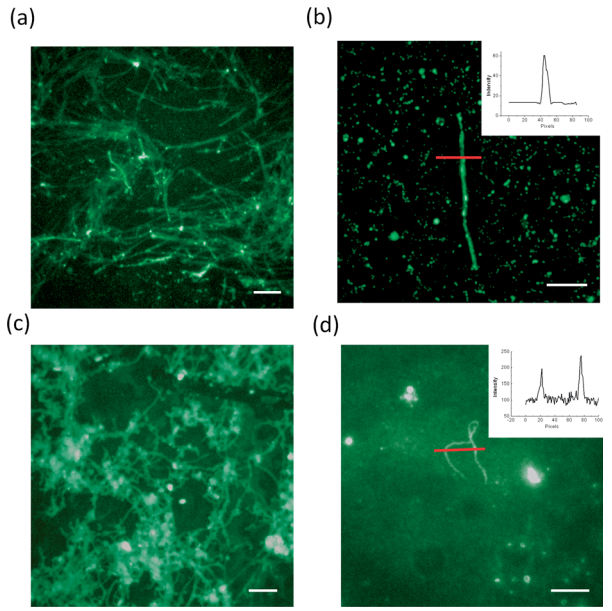

Fig. 4 (a) Fluorescence image of $(PFS^-/PFS^+)_{AI}$-QD nanotubes; (b) fluorescence image of a single $(PFS^-/PFS^+)_{AI}$-QD nanotube, the inset image is the fluorescence intensity profile; (c) fluorescence image of $(PFS^-/PFS^+)_{AI}$-Alexa nanotubes; (d) fluorescence image of a single (PFS^-/PFS^+)-Alexa nanotube, the inset image is the fluorescence intensity profile. Scale bar = 2 μm for all images.

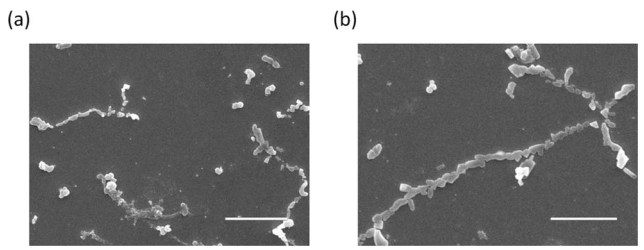

Fig. 6 SEM images of a PFS nanotube structure as observed in 300 min of the electrochemical oxidation process. Scale bar = 5 μm for all images.

obvious tubular structures observed by SEM indicating the validity of this interpretation.

Conclusions

The template assisted LbL technique has been used to fabricate new types of redox stimulus responsive nanotubes. This strategy allows one to achieve a high level of control over the inner diameter and the wall thickness in the fabricated structures by tuning the number of deposited layers. Control over the length and the outer tube diameter can be achieved by the proper choice of the template. Various components such as inorganic particles and organic dye molecules were decorated on the inner surface of the tubes. Tubes were fabricated using PFS redox components and composite mixtures consisting of PFS and PAA. As a model cargo, dye labeled dextran molecules and negatively charged quantum dots were studied. Electrochemically controlled release of these model guests was demonstrated upon electrochemical stimulation of the nanotubes, providing opportunities for molecular delivery applications.

Acknowledgements

We are grateful to A*STAR (Agency for Science, Technology and Research), Singapore and NKTH—A*STAR (Hungarian—Singaporean) Bilateral S&T International Cooperation (BIOSPONA) TeT-08-SG-STAR and to the MESA+ Institute for Nanotechnology of the University of Twente for providing financial support.

Notes and references

1 S. Iijima, *Nature*, 1991, **354**, 56.
2 Q. He, Y. Cui, S. Ai, Y. Tian and J. Li, *Curr. Opin. Colloid Interface Sci.*, 2009, **14**, 115.
3 T. Komatsu, *Nanoscale*, 2012, **4**, 1910.
4 M. Steinhart, *Adv. Polym. Sci.*, 2008, **220**, 123.
5 Y. Cho, W. Lee, Y. K. Jhon, J. Genzer and K. Char, *Small*, 2010, **6**, 2683.
6 P. Avouris, M. Freitag and V. Perebeinos, *Nat. Photonics*, 2008, **2**, 341.
7 R. H. Baughman, A. A. Zakhidov and W. A. de Heer, *Science*, 2002, **297**, 787.
8 J. M. Planeix, N. Coustel, B. Coq, V. Brotons, P. S. Kumbhar, R. Dutartre, P. Geneste, P. Bernier and P. M. Ajayan, *J. Am. Chem. Soc.*, 1994, **116**, 7935.
9 T. D. Lazzara, K. Lau, A. I. bou-Kandil, A. M. Caminade, J. P. Majoral and W. Knoll, *ACS Nano*, 2010, **4**, 3909.
10 C. L. Feng, X. Zhong, M. Steinhart, A. M. Caminade, J. P. Majoral and W. Knoll, *Adv. Mater.*, 2007, **19**, 1933.
11 W. Yuan, Z. Lu, J. Liu, H. Wang and C. M. Li, *Nanotechnology*, 2013, **24**, 045605.
12 C. L. Feng, X. H. Zhong, M. Steinhart, A. M. Caminade, J. P. Majoral and W. Knoll, *Small*, 2008, **4**, 566.
13 Y. Geng, P. Dalhaimer, S. Cai, R. Tsai, M. Tewari, T. Minko and D. E. Discher, *Nat. Nanotechnol.*, 2007, **2**, 249.
14 T. Komatsu, X. Qu, H. Ihara, M. Fujihara, H. Azuma and H. Ikeda, *J. Am. Chem. Soc.*, 2011, **133**, 3246.
15 N. W. S. Kam, Z. A. Liu and H. J. Dai, *Angew. Chem., Int. Ed.*, 2006, **45**, 577.
16 M. Prato, K. Kostarelos and A. Bianco, *Acc. Chem. Res.*, 2008, **41**, 60.
17 J. H. Park, S. Kim and A. J. Bard, *Nano Lett.*, 2006, **6**, 24.
18 A. Thess, R. Lee, P. Nikolaev, H. J. Dai, P. Petit, J. Robert, C. H. Xu, Y. H. Lee, S. G. Kim, A. G. Rinzler, D. T. Colbert, G. E. Scuseria, D. Tomanek, J. E. Fischer and R. E. Smalley, *Science*, 1996, **273**, 483.
19 Y. Wang, A. S. Angelatos and F. Caruso, *Chem. Mater.*, 2008, **20**, 848.
20 Y. N. Xia, P. D. Yang, Y. G. Sun, Y. Y. Wu, B. Mayers, B. Gates, Y. D. Yin, F. Kim and Y. Q. Yan, *Adv. Mater.*, 2003, **15**, 353.
21 J. Landoulsi, S. Moustier-Champagne and C. Dupont-Gillain, *Soft Matter*, 2011, **7**, 3337.
22 J. C. Hulteen and C. R. Martin, *J. Mater. Chem.*, 1997, **7**, 1075.
23 Y. C. Pu, J. R. Hwu, W. C. Su, D. B. Shieh, Y. Tzeng and C. S. Yeh, *J. Am. Chem. Soc.*, 2006, **128**, 11606.
24 G. Che, B. B. Lakshmi, C. R. Martin, E. R. Fisher and R. S. Ruoff, *Chem. Mater.*, 1998, **10**, 260.
25 A. Huczko, *Appl. Phys. A: Mater. Sci. Process.*, 2000, **70**, 365.
26 C. N. R. Rao, B. C. Satishkumar, A. Govindaraj and M. Nath, *ChemPhysChem*, 2001, **2**, 78.
27 Y. G. Sun and Y. N. Xia, *Adv. Mater.*, 2004, **16**, 264.
28 Y. Huang, X. F. Duan, Q. Q. Wei and C. M. Lieber, *Science*, 2001, **291**, 630.
29 L. Zhang, A. Vidyasagar and J. L. Lutkenhaus, *Curr. Opin. Colloid Interface Sci.*, 2012, **17**, 114.
30 M. Raoufi, D. Tranchida and H. Schönherr, *Langmuir*, 2012, **28**, 10091.
31 J. Landoulsi, C. J. Roy, C. Dupont-Gillain and S. Demoustier-Champagne, *Biomacromolecules*, 2009, **10**, 1021.
32 Z. J. Liang, A. S. Susha, A. M. Yu and F. Caruso, *Adv. Mater.*, 2003, **15**, 1849.
33 G. Lu, S. F. Al and J. B. Li, *Langmuir*, 2005, **21**, 1679.
34 Y. Tian, Q. He, Y. Cui and J. Li, *Biomacromolecules*, 2006, **7**, 2539.
35 C. J. Roy, N. Chorine, B. G. De Geest, S. De Smedt, A. M. Jonas and S. Demoustier-Champagne, *Chem. Mater.*, 2012, **24**, 1562.
36 O. Azzaroni and K. Lau, *Soft Matter*, 2011, **7**, 8709.
37 X. Hou, H. Zhang and L. Jiang, *Angew. Chem., Int. Ed.*, 2012, **51**, 5296.
38 J. P. DeRocher, P. Mao, J. Y. Kim, J. Han, M. F. Rubner and R. E. Cohen, *ACS Appl. Mater. Interfaces*, 2012, **4**, 391.
39 N. Du, H. Zhang and D. R. Yang, *Nanoscale*, 2012, **4**, 5517.
40 K. K. Chia, M. F. Rubner and R. E. Cohen, *Langmuir*, 2009, **25**, 14044.
41 L. Han, L. F. Wang, K. K. Chia, R. E. Cohen, M. F. Rubner, M. C. Boyce and C. Ortiz, *Adv. Mater.*, 2011, **23**, 4667.
42 S. A. Sukhishvili, *Curr. Opin. Colloid Interface Sci.*, 2005, **10**, 37.
43 B. G. De Geest, N. N. Sanders, G. B. Sukhorukov, J. Demeester and S. C. De Smedt, *Chem. Soc. Rev.*, 2007, **36**, 636.
44 M. Delcea, H. Möhwald and A. G. Skirtach, *Adv. Drug Delivery Rev.*, 2011, **63**, 730.
45 A. S. Angelatos, B. Radt and F. Caruso, *J. Phys. Chem. B*, 2005, **109**, 3071.

46 M. V. Kiryukhin, S. R. Gorelik, S. M. Man, G. S. Subramanian, M. N. Antipina, H. Y. Low and G. B. Sukhorukov, *Macromol. Rapid Commun.*, 2013, **34**, 87.
47 M. N. Antipina and G. B. Sukhorukov, *Adv. Drug Delivery Rev.*, 2011, **63**, 716.
48 D. J. Schmidt, J. S. Moskowitz and P. T. Hammond, *Chem. Mater.*, 2010, **22**, 6416.
49 A. S. Abd-EI-Aziz and I. Manners, in *Frontiers in Transition Metal-Containing Polymers*, John Wiley & Sons, New Jersey, 2007.
50 J. C. Eloi, D. A. Rider, G. Cambridge, G. R. Whittell, M. A. Winnik and I. Manners, *J. Am. Chem. Soc.*, 2011, **133**, 8903.
51 X. S. Wang, H. Wang, N. Coombs, M. A. Winnik and I. Manners, *J. Am. Chem. Soc.*, 2005, **127**, 8924.
52 M. A. Hempenius, F. F. Brito and G. J. Vancso, *Macromolecules*, 2003, **36**, 6683.
53 D. Jańczewski, J. Song, E. Csanyi, L. Kiss, P. Blazso, R. L. Katona, M. A. Deli, G. Gros, J. W. Xu and G. J. Vancso, *J. Mater. Chem.*, 2012, **22**, 6429.
54 Y. J. Ma, W. F. Dong, M. A. Hempenius, H. Möhwald and G. J. Vancso, *Nat. Mater.*, 2006, **5**, 724.
55 Y. J. Ma, W. F. Dong, M. A. Hempenius, H. Möhwald and G. J. Vancso, *Angew. Chem., Int. Ed.*, 2007, **46**, 1702.
56 J. Song, D. Jańczewski, Y. J. Ma, M. A. Hempenius, J. W. Xu and G. J. Vancso, *J. Mater. Chem. B*, 2013, **1**, 828.
57 J. Song, D. Jańczewski, Y. J. Ma, L. van Lngen, E. S. Ching, Q. L. Goh, J. W. Xu and G. J. Vancso, *Eur. Polym. J.*, 2013, **405**, 256.
58 Z. Wang, G. A. Ozin and I. Manners, *ACS Symp. Ser.*, 2006, **928**, 334.
59 F. Fleischhaker, A. C. Arsenault, Z. Wang, V. Kitaev, F. C. Peiris, G. von Freymann, I. Manners, R. Zentel and G. A. Ozin, *Adv. Mater.*, 2005, **17**, 2455.
60 D. Jańczewski, N. Tomczak, M. Y. Han and G. J. Vancso, *Eur. Polym. J.*, 2009, **45**, 1912.
61 D. Jańczewski, N. Tomczak, M. Y. Han and G. J. Vancso, *Nat. Protoc.*, 2011, **6**, 1546.
62 Y. J. Ma, M. A. Hempenius and G. J. Vancso, *J. Inorg. Organomet. Polym. Mater.*, 2007, **17**, 3.

